Density Fluctuation Measurements Using a Frequency Hopping Reflectometer in JT-60U

Naoyuki OYAMA, Hidenobu TAKENAGA, Takahiro SUZUKI, Yoshiteru SAKAMOTO, Akihiko ISAYAMA and the JT-60 Team

Japan Atomic Energy Agency, 801-1 Muko-yama, Naka, Ibaraki 311-0193, Japan

(Received 24 December 2010 / Accepted 11 February 2011)

In JT-60U, a frequency hopping reflectometer has been developed to evaluate the poloidal rotation velocity as a Doppler reflectometer and the radial correlation of density fluctuations in plasmas. The system can measure the radial profile of density fluctuations or the radial correlation profile at two spatial points within 250 ms by combining with the other fixed frequency reflectometer. The radial profiles of the poloidal rotation velocity evaluated from the Doppler-shifted frequency spectrum of density fluctuations show a positive radial electric field in co-rotating plasmas and a negative radial electric field in counter-rotating plasmas. Density fluctuation measurement at the internal transport barrier (ITB) using a correlation reflectometer revealed that long-range correlation increased when ITB was degraded owing to the central heating by electron cyclotron waves.

Keywords: reflectometer, density fluctuation, radial correlation length, radial electric field, plasma rotation

DOI: 10.1585/pfr.6.1402014

1. Introduction

In JT-60U, the confinement properties and onset conditions of the internal transport barrier (ITB) in weak positive magnetic shear, and weak and strong reversed magnetic shear plasmas have been studied [1, 2]. Although the turbulence suppression by $E \times B$ shear is believed to play an important role in ITB formation [3], the relationship among ITB performance, $E \times B$ shear, and the characteristics of plasma turbulence is not fully understood. Thus, microwave reflectometer systems using O-mode and X-mode propagation have been developed [4, 5]. In a previous study using a three-channel fixed-frequency reflectometer system, no drastic change in the frequency spectrum was observed during the ITB formation phase, and broadband density fluctuations still existed in the ITB region even after a box-type ITB formed [6]. On the other hand, a considerable reduction in the correlation length of the reflectometer signal was observed after the ITB formation without a clear change in the fluctuation amplitude [7].

To evaluate the E_r profile, charge exchange recombination spectroscopy (CXRS) has been used in many devices based on the radial force balance equation [8]. However, poloidal rotation measurement using CXRS in high-temperature plasmas requires some corrections (e.g., for the gyro-orbits effect [9]), and the correction scheme is still being developed. Therefore, the neoclassical poloidal rotation velocity has been used to analyze the JT-60U data so far [3].

For further investigations of the physical mechanism related to transport and turbulence, a new frequency hopping reflectometer has been developed; it can be used as a Doppler reflectometer for E_r profile measurements and as a correlation reflectometer. To confirm its capability, the frequency hopping reflectometer system has been applied to measure E_r profiles in ELMy H-mode plasmas and radial correlation in weak shear plasmas with an ITB in JT-60U.

This paper describes new frequency hopping reflectometer and its application to density fluctuation measurements in JT-60U. Section 2 describes the hardware of the frequency hopping reflectometer. Initial trials of E_r measurement and radial correlation measurement at ITB are presented in Sec. 3. A summary is given in Sec. 4.

2. Frequency Hopping Reflectometer

Several frequency hopping reflectometer systems have been developed and applied to density fluctuation measurements in many devices [10–12]. In these systems, a synthesizer with a frequency of 8-18 GHz is used as a microwave source, and the output of the synthesizer is multiplied by an active multiplier to obtain the required frequency for the measurement. Although the basic configuration of the frequency hopping reflectometer for JT-60U is similar to that of other devices, the synchronized synthesizer developed for JT-60U has some features suitable for remote operation.

Figure 1 shows a schematic of the millimeter-wave section of the frequency hopping reflectometer using the synchronized synthesizer. The synthesizer consists of two sets of a phase-locked loop (PLL) frequency stabilizer and an oscillator at 8-13 GHz. The operation parameters of the synthesizer, such as the frequency and the width (duration)

author's e-mail: oyama.naoyuki@jaea.go.jp

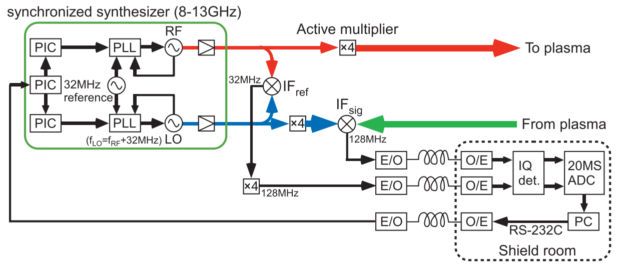

Fig. 1 Schematic of the millimeter-wave section of the frequency hopping reflectometer. Thick arrows show waveguide transmission lines, and thin arrows show coaxial cables.

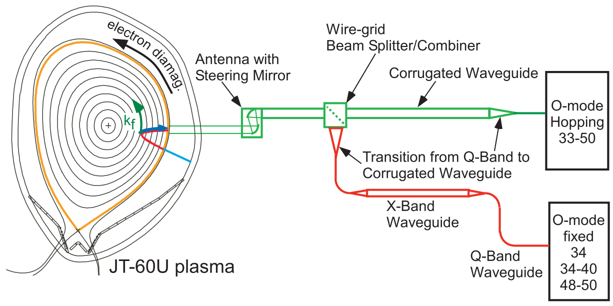

Fig. 2 Schematic of the millimeter-wave transmission line together with the three-channels fixed-frequency O-mode reflectometer system. Two probe waves, one from each reflectometer system, are combined/split by a wire-grid beam combiner/separator. Red line in the plasma shows the result of ray tracing with a frequency of 49.5 GHz in E49534 (see Fig. 5).

of each stair step, can be set in programmable ICs (PICs) using the RS-232C protocol from the shield room through the optical fiber link system. The maximum number of steps is 20. The phase noise of the synthesizer is typically −60 dBc/Hz at 50 kHz, which is an important parameter of the source before frequency multiplication. For heterodyne detection, a frequency difference of 32 MHz between the two oscillators is automatically established by two PLL frequency stabilizers.

The main branches of two outputs from the synthesizer are fed to active frequency multipliers (×4) to obtain a probe wave (+16 dBm) and a reference wave (+10 dBm) in the Q-band (33-50 GHz). The reflected wave from the plasma and the reference wave provide a 128 MHz IF$_{sig}$ signal. The low-power reference branches from the outputs of the synthesizer divided by directional couplers provide a 32 MHz IF$_{ref}$ signal. The IF$_{ref}$ signal is fed to another active frequency multiplier (×4), and then both IF$_{sig}$ and IF$_{ref}$ signals at 128 MHz are fed into the quadrature-type phase detector (IQ detector) located in the shield room through the optical fiber link system. All these components (except for the IQ detector) are assembled into two 19-inch rack cases and installed inside the shield box in the torus hall.

The IQ outputs, i.e., the sine and cosine components of the received signal, are acquired by a PC-based 14-bit digitizer (Spectrum M2i.4031), which can digitize two channels of analog data with a sampling rate of 20 Msamples/s up to the maximum size of a hard disk drive system. Thus, the system can measure the density fluctuation through a discharge (5.2 GB/shot for a 65 s discharge at the maximum). To correct the DC offset of the IQ outputs, active terminators using a *p-i-n* diode are inserted at the input of the IQ detector. The controller of the digitizer produces 5 ms gate pulses for the terminator at the beginning of the discharge. In this way, we obtain correction data for the offset calibration for each channel in every discharge.

The probe wave of the frequency hopping reflectometer is combined with other probe waves from the fixed frequency O-mode reflectometers by a wire-grid beam combiner and then launched into the plasma as shown in Fig. 2.

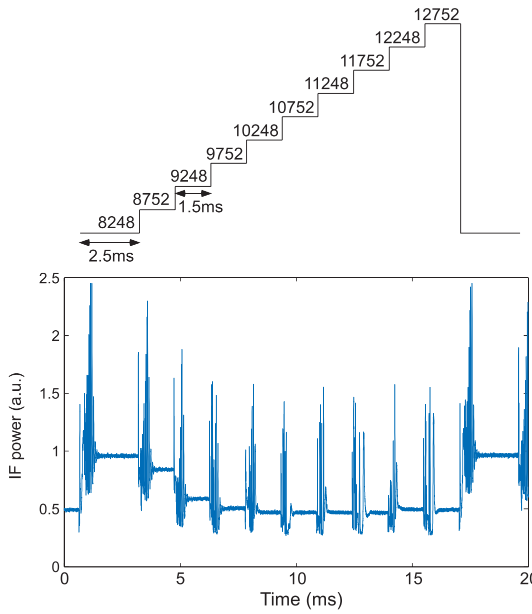

Fig. 3 Characteristics of pull-in time of the synthesizer during fast frequency hopping. Upper figure shows a staircase launch frequency pattern in units of MHz for full band hopping. Lower figure shows the time evolution of the IF power with a frequency of 32 MHz.

The antennas for the incident and received waves are located at $Z = 0.1$ m, and the injection angle of the probe wave is fixed at zero degrees (horizontal injection) in a typical experiment. When the system is used as a Doppler reflectometer, the plasma position is optimized to avoid the detection of the mirror reflection component. In the case shown in Fig. 2, only scattered waves satisfying the Bragg condition ($k_f = 2k_iN$, where k_f, k_i, and N are the wave number of the density fluctuations, the wave number of the incident wave, and the refractive index at the reflecting point, respectively) can be received by the antenna as shown by the blue arrow. For the correlation measurement, on the other hand, the plasma position is adjusted around $Z = 0.1$ m so that the probe waves are injected perpendicular to the magnetic surface. The received wave is fed into a Q-band bandpass filter to reject high-power microwaves used for electron cyclotron heating (ECH) at 110 GHz and then fed into the Q-band mixer to obtain $\mathrm{IF}_{\mathrm{sig}}$.

The reflectometer system can operate precisely only when the two oscillators in the synthesizer are synchronized while maintaining a 32 MHz frequency difference. To evaluate the dead time for each stair step, the typical pull-in time of the synthesizer has been tested using an X-band mixer, a 32 MHz bandpass filter, and a video detector. As shown in Fig. 3, the IF power was fluctuated just after frequency hopping owing to unlocking of PLL stabilizer. Typically, 500 μs after hopping (700 μs at the maximum), the two oscillators can be synchronized. Based on this result, each frequency step is typically held constant for 20 ms, and 13 steps are used for typical profile measurements, including 1 marker step. Thus, about 250 ms is required for each sweep.

Table 1 Frequency and cutoff density of each step in Doppler reflectometer.

step	frequency (GHz)	Cutoff density (10^{19} m^{-3})
1	33.5	1.40
2	35.3	1.55
3	37.0	1.70
4	38.6	1.85
5	40.1	2.00
6	41.6	2.15
7	43.0	2.30
8	44.4	2.45
9	45.7	2.60
10	47.0	2.74
11	48.3	2.90
12	49.5	3.05

3. Experimental Results

3.1 E_{r} profile measurement using Doppler reflectometer

The principle of Doppler reflectometry and its application to the $v_\perp(E_{\mathrm{r}})$ profile measurement can be found elsewhere [13, and references therein]. A fundamental requirement of a Doppler reflectometer is the geometrical arrangement of the antenna against the cutoff density layer. In JT-60U, as described above, the plasma position is adjusted so as to receive only scattered waves satisfying the Bragg condition and so that the frequency hopping reflectometer system acts as a Doppler reflectometer. Because the wavenumber of density fluctuations perpendicular to the magnetic field line $k_\perp$ is typically much larger than the other components, $k_\parallel$ and k_{r}, in tokamak plasmas (i.e., $k_\perp \sim k_{\mathrm{f}}$), the Doppler shift frequency f_{D} of the density fluctuation is expressed as $f_{\mathrm{D}} = Nk_{\mathrm{i}}v_\perp/\pi$, where $v_\perp$ is the component of the turbulence velocity perpendicular to the magnetic field line.

The initial E_{r} profile measurements using the Doppler reflectometer were performed in ELMy H-mode discharges with a plasma current (I_{p}) of 1.6 MA and a toroidal magnetic field (B_{T}) of 3.5 T. One second after the main heating, the combination of tangential neutral beam injection (NBI) units was changed from balanced injection to co- or counter-dominated injection at $t = 7$ s. The toroidal rotation at r/a~0.6 increased in the co- or counter-direction as shown in Figs. 4 and 5. Here, the positive toroidal rotation means co-direction to the plasma current.

In these discharges, 12 frequency-hopping steps (Table 1) were applied. The frequency change corresponding to each sweep can be seen in the spectrogram of density fluctuations as shown in Figs. 4 (c) and 5 (c). When the toroidal rotation became faster in the counter-direction, the peak frequency in the spectrogram moved in the negative direction as shown in Fig. 5 (c). Figures 4 (d) and 5 (d) compare the frequency spectrum of density fluctuations measured with the innermost channel (at the highest frequency of 49.5 GHz). In both cases, f_{D} can be determined by a fitting function, which is expressed as $\alpha \exp(-(f - f_{\mathrm{D}})^2/\sigma^2)$. Here, α and σ are fitting coefficients. It is noted that the sign of the Doppler shift changed when the sign of the toroidal rotation changed, indicating that the sign of $v_\perp$ changed. By applying the same analysis to each frequency step, the radial profile of f_{D} is obtained, as shown in Fig. 7 by using the electron density (n_{e}) profile shown in Fig. 6 (a).

The measured $v_\perp$ contains two components: phase velocity of the density fluctuation (v_{phase}) and $E\times B$ velocity of the plasma ($v_{E\times B}$), i.e., $v_\perp = v_{\mathrm{phase}} + v_{E\times B}$. Because v_{phase} has not been measured directly in JT-60U, the condition of the $v_{E\times B} \gg v_{\mathrm{phase}}$ is assumed to be similar to those of other studies [13, 14]. Then, we obtain the relationship between $v_{E\times B}$ and f_{D} as $v_{E\times B} = cf_{\mathrm{D}}/(2fN)$ (where f is the frequency of the incident wave, and c is the velocity of light). In our analysis, N and the scattering point (R and Z) are evaluated by a ray-tracing code [15] using actual plasma equilibrium and plasma profiles. Finally, E_{r} can be evaluated using the total magnetic field at the scattering region (B_{total}) as $E_{\mathrm{r}} = v_{E\times B}B_{\mathrm{total}}$ [8].

The symbols in Fig. 7 (b) represent the radial profile of E_{r} in co- and counter-rotating plasmas. At the edge region near the top of the pedestal ($r/a \sim 0.9$), negative E_{r} values produced by the steep pressure gradient at the H-mode pedestal were observed in both the co- and counter-rotating cases. This level of negative E_{r} has been observed near the top of the pedestal [16]. In the core region ($r/a \sim 0.6$), positive E_{r} was observed in a co-rotating plasma (E49535). A change in the sign of E_{r} from negative to positive across the top of the pedestal has often been observed in many

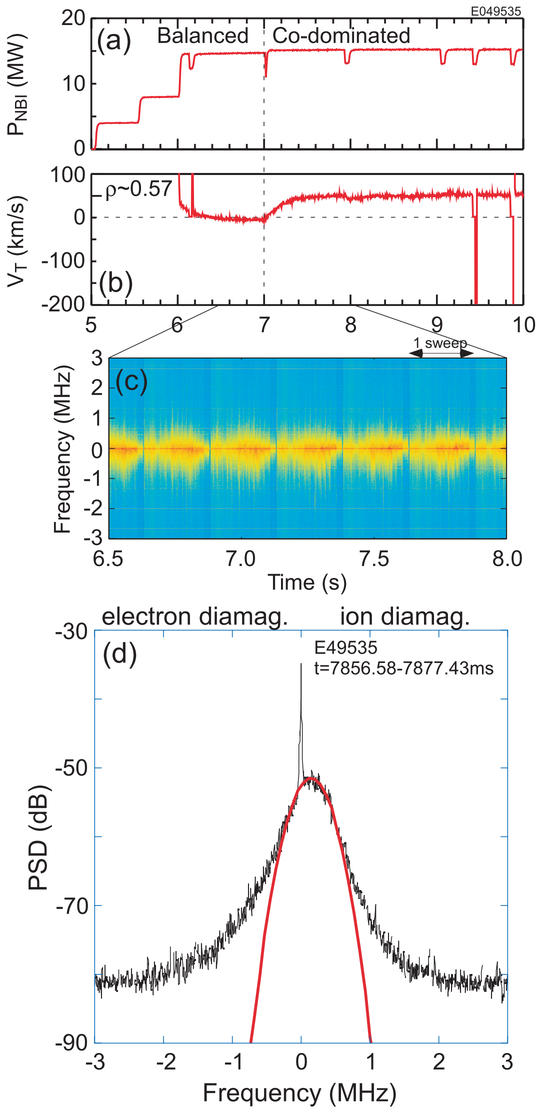

Fig. 4 Waveforms of (a) NBI power and (b) toroidal rotation measured with charge exchange recombination spectroscopy when balanced NBIs are changed to co-dominated NBIs. (c) Spectrogram of density fluctuation measured on the Doppler reflectometer. (d) Frequency spectrum of density fluctuation at 49.5 GHz (n_c = 3.05×10^{19} m^{-3}). Orange line shows the fitting line for determining f_D. Negative frequency means that density fluctuation propagates in the electron diamagnetic drift direction.

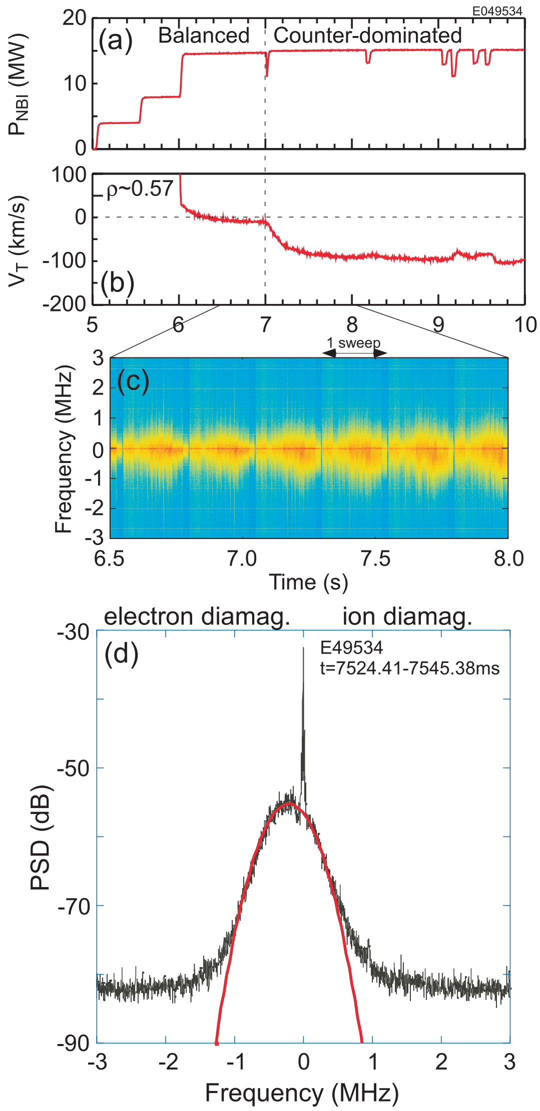

Fig. 5 Waveforms of (a) NBI power and (b) toroidal rotation measured with charge exchange recombination spectroscopy when balanced NBIs are changed to counter-dominated NBIs. (c) Spectrogram of density fluctuation measured on the Doppler reflectometer. (d) Frequency spectrum of density fluctuation at 49.5 GHz (n_c = 3.05×10^{19} m^{-3}). Orange line shows the fitting line for determining f_D. Negative frequency means that density fluctuation propagates in the electron diamagnetic drift direction.

tokamaks [8]. In the co-rotating plasma, the evaluated E_r profile is consistent with that evaluated by the radial force balance equation assuming neoclassical poloidal rotation as shown in Fig. 7. However, the absolute value of E_r in the counter-rotating plasma is different from that evaluated by the radial force balance equation. Because the discrepancy is large at the edge region, one possible reason is the different level of fast ion losses caused by different orbits of passing fast ions originating from tangential NBIs (i.e., a larger orbit loss was observed with counter-tangential NBIs). Further analysis to understand this discrepancy remains to be investigated as future work.

3.2 Density fluctuation measurement using correlation reflectometer

To investigate the relationship between ITB performance and the plasma turbulence characteristics, the radial correlation of density fluctuations is measured with a correlation reflectometer. The system consists of the frequency hopping reflectometer and fixed-frequency reflectometers [5]. As shown in Fig. 8, the frequencies of the frequency hopping reflectometer are distributed near the

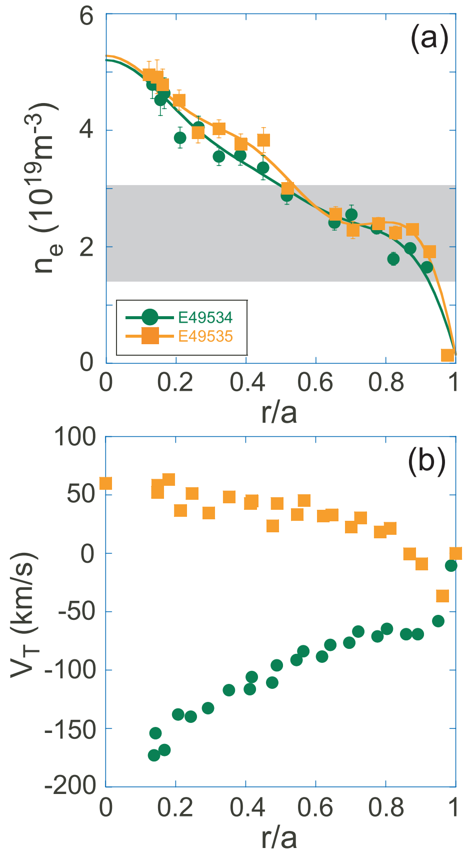

Fig. 6 Comparison of (a) density profile and (b) toroidal rotation profile for E49534 (counter-rotation) and E49535 (co-rotation) at t = 7.5 s. Shaded area in (a) shows measurement region of the Doppler reflectometer (see. Table 1).

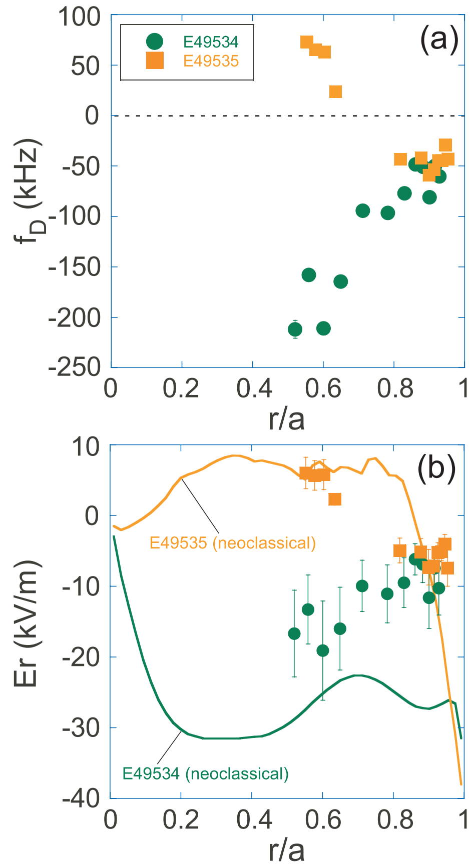

Fig. 7 Comparison of (a) f_D profile and (b) E_r profile for E49534 (counter-rotation) and E49535 (co-rotation). Symbols represent the E_r profile evaluated on the Doppler reflectometer. Lines in (b) represent the E_r profile evaluated by radial force balance equation with neoclassical poloidal rotation.

frequency of two fixed-frequency reflectometers. At each frequency step, the radial distance between the two reflectometer channels is calculated using the electron density and electron temperature profiles (the electron temperature (T_e) is used to correct the relativistic effect of the cut-off condition [17]). Then, to obtain the radial correlation length, the coherence of the two reflectometer signals is plotted as a function of the radial distance between the two reflectometers.

When we plot the coherence of each step, we adopt the averaged coherence of density fluctuations in a certain frequency range. In the case shown in Fig. 9, the highest coherence was found in the frequency range of −100 to −50 kHz. The frequency range was determined using the nearest channels and then the same frequency range was applied to all frequency steps. Note that the frequency spectra shown in Figs. 9 (a) and (b) were nearly symmetrical, in contrast to the frequency spectra of the Doppler reflectometer shown in Figs. 4 and 5, indicating that the geometrical configuration is suitable for a correlation reflectometer.

In JT-60U, the impact of ECH on the ITB has been investigated, and ECH was found to be capable of degrad-

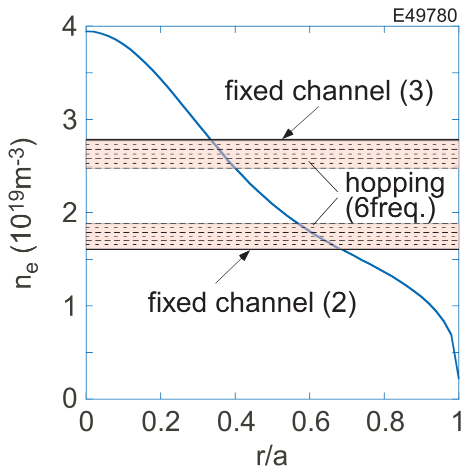

Fig. 8 Density profile and measured density region of the correlation reflectometer (see Table 2).

ing the ion temperature ITB (T_i-ITB) [18]. Because the physical mechanism of this ITB degradation is not understood, the correlation reflectometer system was applied to

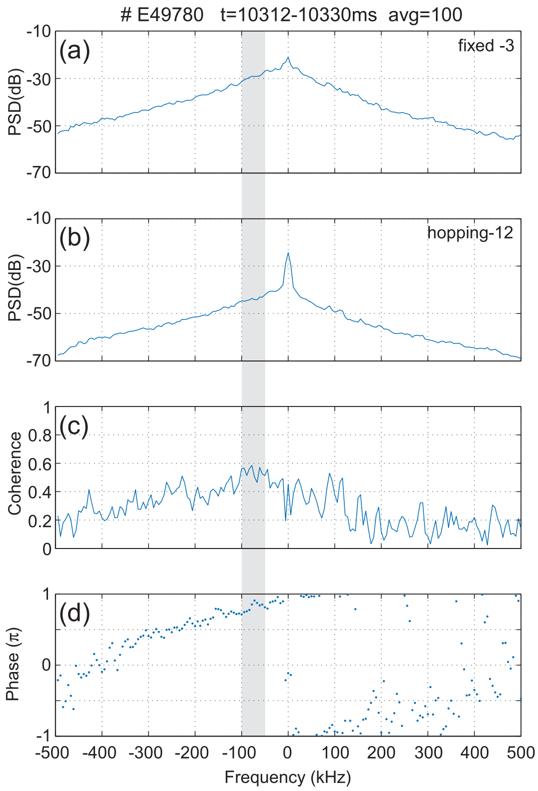

Fig. 9 Example of analysis of radial correlation. (a) and (b) Power spectral density of fixed-frequency channel and hopping channel, respectively, and (c) and (d) coherence and phase, respectively, of the two signals shown in (a) and (b). Ensemble average number was 100.

Table 2 Frequency and cutoff density of each step in correlation reflectometer.

step	frequency (GHz)	Cutoff density (10^{19} m^{-3})
1	36.5	1.66
2	37.0	1.70
3	37.5	1.75
4	38.0	1.79
5	38.5	1.84
6	39.0	1.89
7	44.7	2.48
8	45.1	2.53
9	45.6	2.58
10	46.0	2.63
11	46.5	2.68
12	46.8	2.73
Fixed-2	36.0	1.61
Fixed-3	47.3	2.78

JT-60U weak shear plasmas with T_i-ITB [19]. Considering the density profile near the measured points of two fixed-frequency reflectometers, the frequency at each of the 12 steps is carefully determined as summarized in Table 2.

In a weak shear plasma with I_p = 1.2 MA and B_T = 3.7 T (E49780), the central T_i decreased during the application of central ECH (the absorption location was r/a < 0.3) as shown in Fig. 10. Immediately after the injection of ECH, the central T_e started to increase together with the reduction of n_e. About 100 ms later, the central T_i decreased together with the change in the density fluctuation as shown in Fig. 10 (e). Figure 10 (g) compares the coherence of density fluctuations with and without ECH, indicating that the long-range correlation (> ∼2 cm) increased. In this discharge, the density profile changed so that the density gradient near the measured location became smaller. However, the change in the characteristics of the density fluctuations was not correlated with the change in the density profile but with the degradation of T_i-ITB.

To understand the relationship between the changes in the density profile and radial correlation, the correlation reflectometer was applied to another weak shear plasma with I_p = 1.5 MA and B_T = 3.7 T (E48973), where T_i-ITB was maintained during the application of central ECH. As shown in Fig. 11, the central T_i and T_e were constant or increased slightly after ECH injection, whereas the central n_e gradually decreased; as a result, the density gradient near the measured location decreased. As the density profile changed, the shape of the frequency spectrum measured with the fixed-frequency reflectometer, shown in Fig. 11 (e), peaked gradually during ECH. This type of gradual change in the shape of the frequency spectrum was also observed in the T_i-ITB degradation case shown in Fig. 10 (e). However, the radial correlation of the density fluctuations was almost constant. These experimental observations indicate that the observed change in the radial correlation is caused not by the change in the density profile but by the change in the characteristics of the density fluctuations.

4. Summary

A frequency hopping reflectometer using a synchronized synthesizer has been developed for use as a Doppler reflectometer and correlation reflectometer in JT-60U. The synchronized synthesizer provides a fast sweep of the frequency of the probe wave so that 13 varied frequency steps can be typically applied every 250 ms. The system has been applied to density fluctuation measurements to evaluate the E_r profile or the radial correlation of density fluctuations. When it was applied as a Doppler reflectometer, radial profiles of the poloidal rotation velocity evaluated from the Doppler-shifted frequency spectrum of density fluctuations showed a positive radial electric field in a co-rotating plasma and a negative radial electric field in a counter-rotating plasma in core plasma (r/a ∼ 0.6). In addition, density fluctuation measurement by the correlation reflectometer in the ITB region revealed that the long-range correlation increased when T_i-ITB was degraded

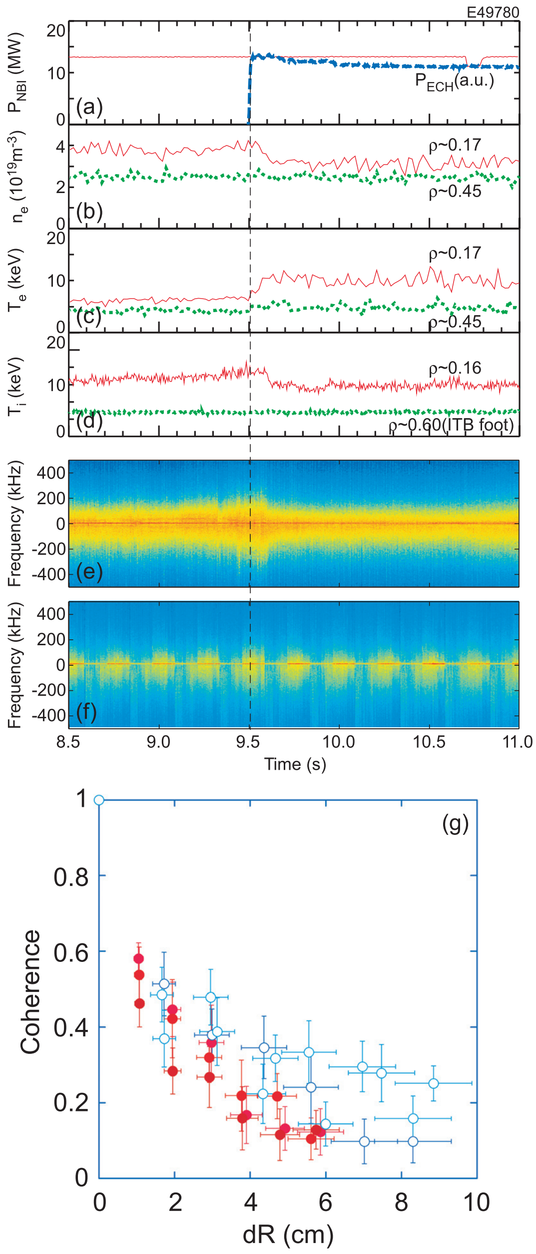

Fig. 10 Typical example of T_i-ITB degradation case. Waveforms of (a) NBI and ECH power, (b) electron density, (c) electron temperature, and (d) ion temperature. (e) Spectrogram of density fluctuation measured on the fixed-frequency reflectometer (47.3 GHz). (f) Spectrogram of density fluctuation measured on the frequency hopping reflectometer. (g) Coherence of density fluctuations at $r/a \sim 0.3$. Open and closed symbols denote data with and without ECH, respectively. Coherence is averaged in a frequency range of -100 to -50 kHz.

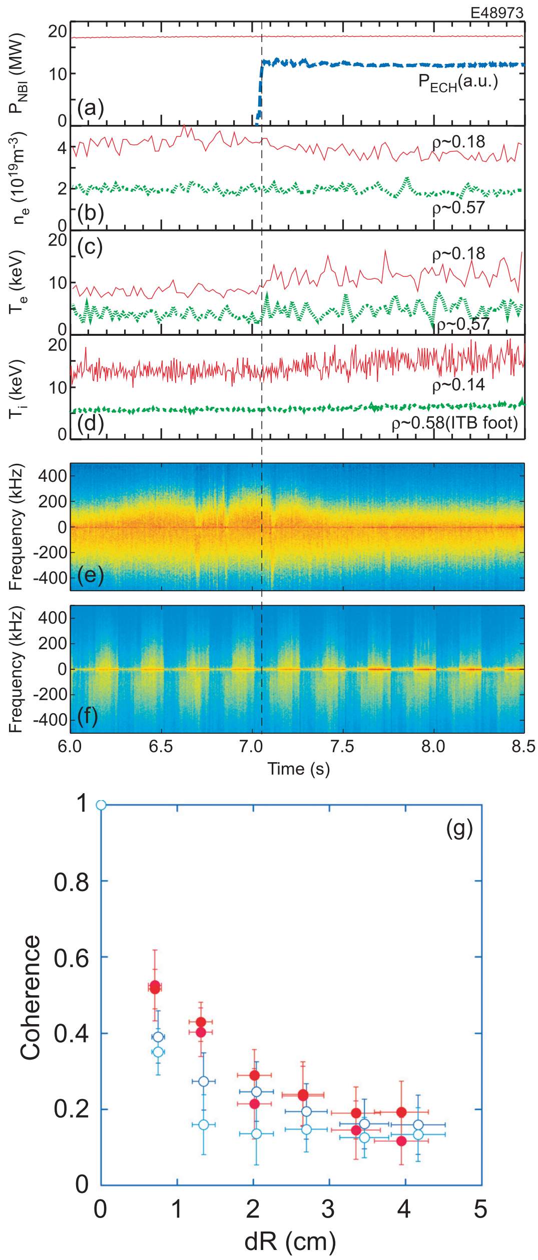

Fig. 11 Typical example of unchanged T_i-ITB case. Waveforms of (a) NBI and ECH power, (b) electron density, (c) electron temperature, and (d) ion temperature. (e) Spectrogram of density fluctuation measured on the fixed-frequency reflectometer (47.3 GHz). (f) Spectrogram of density fluctuation measured on the frequency hopping reflectometer. (g) Coherence of density fluctuations at $r/a \sim 0.3$. Open and closed symbols denote data with and without ECH, respectively. Coherence is averaged in a frequency range of -100 to -50 kHz.

owing to central heating by ECH. Further analysis under various experimental conditions will provide useful information regarding the relationship among the anomalous transport, $E\times B$ shear, and density fluctuations.

Acknowledgments

The authors acknowledge the members of the Japan Atomic Energy Agency who have contributed to the JT-60U projects. The authors are grateful to Drs. M. Kikuchi and M. Mori for continuous encouragement and support. This research was supported by the Grant-in-Aid for

Young Scientists (A) 18686076, Japan Society for the Promotion of Science.

[1] Y. Sakamoto, T. Suzuki, S. Ide *et al.*, Nucl. Fusion **44**, 876 (2004).
[2] H. Takenaga, S. Higashijima, N. Oyama *et al.*, Nucl. Fusion **43**, 1235 (2003).
[3] H. Shirai, M. Kikuchi, T. Takizuka *et al.*, Nucl. Fusion **39**, 1713 (1999).
[4] K. Shinohara, R. Nazikian, T. Fujita and R. Yoshino, Rev. Sci. Instrum. **70**, 4246 (1999).
[5] N. Oyama and K. Shinohara, Rev. Sci. Instrum. **73**, 1169 (2002).
[6] N. Oyama, L.G. Bruskin, H. Takenaga *et al.*, Plasma Phys. Control. Fusion **46**, A355 (2004).
[7] R. Nazikian, K. Shinohara, G.J. Kramer *et al.*, Phys. Rev. Lett. **94**, 135002 (2005).
[8] K. Ida, Plasma Phys. Control. Fusion **40**, 1429 (1998).
[9] R.E. Bell and E.J. Synakowski, AIP Conference Proceedings **547**, 39 (2000).
[10] T. Estrada, E. Blanco, L. Cupido, M.E. Manso and J. Sánchez, Nucl. Fusion **46**, S792 (2006).
[11] S. Graca, G.D. Conway, P. Lauber *et al.*, Plasma Phys. Control. Fusion **49**, 1849 (2007).
[12] T. Tokuzawa, A. Ejiri and K. Kawahata, Rev. Sci. Instrum. **81**, 10D906 (2010).
[13] G.D. Conway, J. Schirmer, S. Klenge *et al.*, Plasma Phys. Control. Fusion **46**, 951 (2004).
[14] M. Hirsch, E. Holzhauer, J. Baldzuhn, B. Kurzan and B. Scott, Plasma Phys. Control. Fusion **43**, 1641 (2001).
[15] K. Hamamatsu and A. Fukuyama, Plasma Phys. Control. Fusion **42**, 1309 (2000).
[16] K. Kamiya, K. Ida, Y. Sakamoto *et al.*, Phys. Rev. Lett. **105**, 045004 (2010).
[17] E. Mazzucato, Phys. Fluids B **4**, 3460 (1992).
[18] S. Ide, H. Takenaga, A. Isayama *et al.*, Nucl. Fusion **47**, 1499 (2007).
[19] H. Takenaga, N. Oyama, H. Urano *et al.*, Nucl. Fusion **49**, 075012 (2009).